Theoretical investigation into tunable band gaps of an Euler- Bernoulli beam with 2DOF LR structures

Theoretical investigation into tunable band gaps of an Euler-Bernoulli beam with 2DOF LR structures

Zhao Xingqian[1,2] Shuai Changgeng[1,2] Gao Yan[3] Emiliano Rustighi[4]
[1] Institute of Noise & Vibration, Naval University of Engineering, Wuhan, P.R.China
[2] National Key Laboratory of Ship Vibration and Noise, Wuhan, P.R.China
[3] Key Laboratory of Noise and Vibration Research, Institute of Acoustics, Chinese Academy of Science, P.R. China
[4] Institute of Sound and Vibration Research, University of Southampton, U.K.

E-mail: xqzhao0613@163.com

Abstract. This paper is concerned with an intelligent phonotic crystals (IPC) consisting of an Euler-Bernoulli beam attached with 2DOF locally resonant (LR) structures. The novel design of the dielectric electroactive polymer (DEAP) rings acting as the springs of oscillators is presented that could be employed to control the transmission of flexural waves on the beam. Tunable band gaps (BGs) can be realized by changing the stiffness of each oscillator driven by the external electric field, where the DEAPs transform electric energy directly into mechanical work under the applied voltage. Discrete copper (Cu) strips are then attached to the DEAP to allow the deformation of DEAP rings. The transfer matrix (TM) theory is adopted to assist readers to better understand the formation of the BG. Simulation results show that this particular configuration is effective for attenuating the flexural waves at low frequencies below 1000Hz where the tunable BGs may occur. Moreover, it is found that a wider BG can be achieved and shifts towards higher frequencies by increasing the applied voltages.

1. Introduction

Over the last decades, the concepts of artificially-structured periodic materials known as phonotic crystals (PCs) and metamaterials, have been introduced to develop novel materials with the property of band gaps (BGs), in which transmission of sound and/or vibration is forbidden [1-3] . As such, these materials are of particular interest and have been proposed as a potential solution for the design of acoustic/elastic filters, noise control, vibration less environments for high-precision mechanical systems and improvement in the design of transducers [4].

In general, there are two types of BGs, including the Bragg BG and the locally resonant (LR) BG [5]. For the conventional Bragg BGs, the BG is caused by the inference of Bragg scattering due to the periodicity or the reaction between unit cells, and thereby the physical dimension of a BG material is typically much larger than the wavelength at the fundamental BG frequencies. This severely restricts the application of Bragg BGs at low frequencies. On the other hand, acoustic/elastic metamaterials as proposed by Liu *et al* [6] have desirable features of realizing BGs at significant lower frequencies due to the resonant behavior exhibited in the materials. Albeit attractive for low frequency applications, the LR BGs are typical limited to fixed and narrow frequency bands. There is an aspiration to provide a

commercially viable solution, in particular, in practical situations where there is a drift of the attenuation band.

Dielectric electroactive polymers (DEAPs) fall into the category of smart materials, and are known to be capable of substantial changes in size or shape subjected to electrical stimulation. Recent research has shown the potential of these materials in actuator applications due to their efficient deformation characteristics, fast response time and high energy densities. The application of DEAPs in PCs have been investigated in recent work [4,7-10]. Here, tunable BGs are achieved by adopting DEAPs acting as the springs of oscillators for the suppression of flexural waves in beam-like structures. This combined structure forms the intelligent phononic crystals (IPCs), with the tunable BG properties governed by the applied voltage in the external electric field.

Yu *et al* [2] studied the flexural vibration band gaps in an Euler-Bernoulli beam with 2 degree-of-freedom (DOF) LR structures. Based on this model, the BG properties in the proposed IPC are investigated. The relationship between the applied voltage and deformation of the proposed structure is established. The transfer matrix (TM) theory is introduced to explain the formation of the BG. The transmission frequency response function (FRF) of the structure with finite length is calculated by the finite element (FE) method. Numerical results demonstrate that tunable BGs contributed by the LR mechanism, can be realized by varying voltages in the external electric field.

2. Relationship between the applied voltage and deformation

The proposed IPC structure can be modelled as an Euler-Bernoulli beam with 2DOF LR structures, as illustrated in Figure 1, with detailed information as described in Figure 2. The beam is constructed from an aluminum tube with the inner and outer radii being r_0=7 and r_1=10mm, respectively. Referring to Figure 2(b), each unit of the LR structure is composed of two soft DEAP rings with outer radius r_2=15mm and equispaced heavy Cu strips attached at the DEAP rings. The radius of the outer layer of strips is r_3=19.5mm. The main advantage of discrete Cu strips over the distributed ring covering outside the DEAP is to allow the deformation of DEAP under the applied voltage. The length of the DEAP ring is h=10mm. The length of the Cu strip is $2l$=60mm and the angle of each strip is b spaced by g between two adjacent strips. The lattice constant is a=1.5×10^{-1}m. The cross-section area of the aluminum beam is calculated as A=1.602×10^{-4}m^2 and the area moment of inertia I=5.986×10^{-9}m^4.

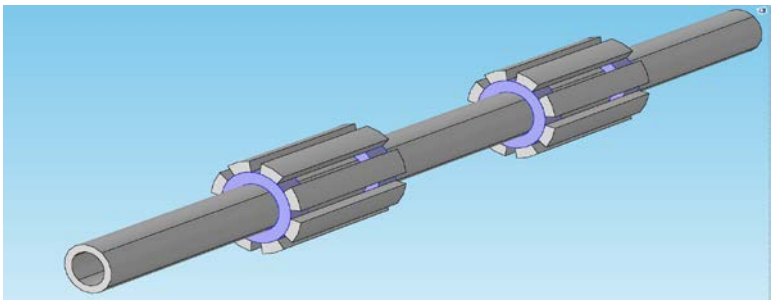

Figure 1. An Euler-Bernoulli beam with 2DOF LR structures.

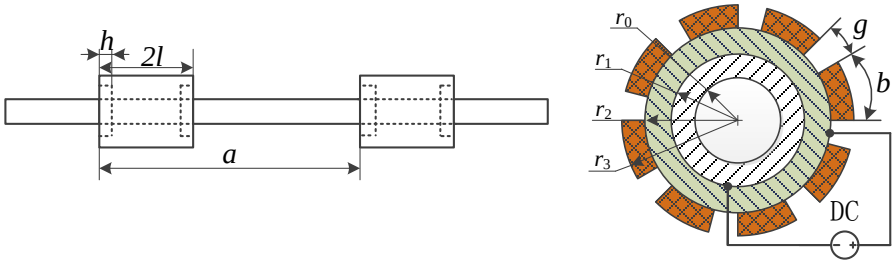

(a) (b)

Figure 2. The schematic design of the IPC structure: (a) in the longitudinal direction; (b) the cross-section.

The analytical relationship between the applied voltage V and the DEAP strains in the radial direction was derived in [9,11]. The model is extended here to study the structure with discrete Cu strips. Important assumptions are made in the analysis as follow,

(1) The elastic analysis is modelled under plane strain conditions;

(2) The DEAP is assumed to be isotropic and its viscoelastic behaviour is ignored;

(3) Small strain and linear deformation are assumed in the calculation.

By applying a voltage between the outer and inner surfaces of the DEAP ring, an electrostatic field arises and the Maxwell's electrostatic pressure from the surface mechanically presses the DEAP ring. As a result of the mechanical compression, the thickness z decreases and thus the radial displacement occurs, which in turn tunes the BGs due to the change in the stiffness of the LR structures. This suggests that the BGs can be tuned by controlling the applied electric field.

The Maxwell's electrostatic pressure p loading on the DEAP ring with thickness z is obtained by [12]

$$p = \varepsilon_0 \varepsilon_r E^2 = \varepsilon_0 \varepsilon_r \left(V/z\right)^2 \tag{1}$$

where ε_0 and ε_r are the free space permittivity and relative permittivity respectively; V is the applied electric voltage. It is noted that the free space permittivity keeps constant, ε_0=8.85×10^{-12}F/m. The electrostatic pressures p_i and p_o, exerted by the inner and outer surfaces, are related to an applied voltage V by [13]

$$p_i = \frac{D\varepsilon_0\varepsilon_r V^2}{2\ln^2\left(r_2/r_1\right)r_1^2 r_2\left(r_2^2 - r_1^2\right)},\ p_o = \frac{D\varepsilon_0\varepsilon_r V^2}{2\ln^2\left(r_2/r_1\right)r_1 r_2^2\left(r_2^2 - r_1^2\right)} \tag{2}$$

and

$$D = \left[r_1^6 + r_2^6 - r_1^2 r_2^4 - r_1^4 r_2^2 + 8\ln\left(r_2/r_1\right)\left(r_2^2 - r_1^2\right)r_1^2 r_2^2 + 4\ln^2\left(r_2/r_1\right)\left(r_2^2 + r_1^2\right)r_1^2 r_2^2\right]^{1/2} \tag{3}$$

For time-invariant displacements and the axisymmetric motion, the equation of compatibility in polar coordinates is [14]

$$\left(\frac{\mathrm{d}^2}{\mathrm{d}r^2} + \frac{1}{r}\frac{\mathrm{d}}{\mathrm{d}r}\right)\left(\frac{\mathrm{d}^2\phi}{\mathrm{d}r^2} + \frac{1}{r}\frac{\mathrm{d}\phi}{\mathrm{d}r}\right) = 0 \tag{4}$$

where ϕ is the Airy stress function, depending only on r. The solution of the above equation is

$$\phi = A\log r + Br^2\log r + Cr^2 + D \tag{5}$$

with the constants A, B, C, D defined by the boundary conditions. The corresponding stress components are given by

$$\sigma_r = \frac{1}{r}\frac{\mathrm{d}\phi}{\mathrm{d}r^2} = \frac{A}{r^2} + B\left(1 + 2\log r\right) + 2C,\ \sigma_\theta = \frac{\mathrm{d}^2\phi}{\mathrm{d}r^2} = -\frac{A}{r^2} + B\left(3 + 2\log r\right) + 2C,\ \tau_{r\theta} = 0 \tag{6}$$

For the uniform internal and external pressure loadings as shown in Figure 3, the stress components become

$$\sigma_r = \frac{A}{r^2} + 2C,\ \sigma_\theta = \frac{\mathrm{d}^2\phi}{\mathrm{d}r^2} = -\frac{A}{r^2} + 2C \tag{7}$$

The boundary conditions of the hollow cylinder are

$$\left(\sigma_r\right)_{r=r_1} = -p_i,\ \left(\sigma_r\right)_{r=r_2} = -p_0 \tag{8}$$

Substituting Eqs. (8) into (7), the constants A and C are found to be

$$A = \frac{r_1^2 r_2^2\left(p_i - p_0\right)}{r_2^2 - r_1^2},\ C = \frac{p_i r_1^2 - p_0 r_2^2}{2\left(r_2^2 - r_1^2\right)} \tag{9}$$

Substituting Eqs. (9) into (7) leads to

$$\sigma_r = \frac{r_1^2 r_2^2 (p_i - p_0)}{r_2^2 - r_1^2}\frac{1}{r^2} + \frac{p_i r_1^2 - p_0 r_2^2}{(r_2^2 - r_1^2)}, \ \sigma_\theta = -\frac{r_1^2 r_2^2 (p_i - p_0)}{r_2^2 - r_1^2}\frac{1}{r^2} + \frac{p_i r_1^2 - p_0 r_2^2}{(r_2^2 - r_1^2)} \tag{10}$$

Given the plane strain condition, the plane stress ε_θ satisfies

$$E\varepsilon_\theta = \sigma_\theta - \upsilon\sigma_r \tag{11}$$

where E and v are the Yong's modulus and Poisson's ratio of the DEAP. The radial displacement u is found from the relationship $\varepsilon_\theta = u/r$, and given by

$$u(r) = r\varepsilon_\theta = \frac{r}{E}(\sigma_\theta - \nu\sigma_r) \tag{12}$$

Substituting Eqs. (10) into (12), the radial displacement (deformation in thickness) is found to be related to the applied voltage by

$$u(r) = \frac{D\varepsilon_0\varepsilon_r r}{2\ln^2(r_2/r_1) r_1 r_2 E(r_2 - r_1)(r_2 + r_1)^2} \times \left[\left(\frac{r_1 r_2}{r^2} + 1\right)(1+\nu) - 2\right]\left(\frac{V}{r_2 - r_1}\right) \tag{13}$$

The deformation in the radial direction is given by

$$\Delta r = u(r_2) - u(r_1) \tag{14}$$

In response to the applied voltage, the inner and outer radii become

$$r_1' = r_1, \ r_2' = r_2 + \Delta r \tag{15}$$

Assuming the volume of the DEAP remain unchanged [11] leads to

$$(\pi r_2^2 - \pi r_1^2)h = (\pi r_2'^2 - \pi r_1^2)h' \tag{16}$$

Combining Eqs. (14)-(16), the deformation in the longitudinal direction is obtained by

$$h' = \frac{h(r_2^2 - r_1^2)}{\left[r_2 + u(r_2) - u(r_1)\right]^2 - r_1^2} \tag{17}$$

Specifically, for a DEAP ring, the radial stiffness can be determined by [15]

$$k = \frac{\pi(5 + 3.29H^2)G_1 h}{\ln(r_2/r_1)} \tag{18}$$

where G_1 are the shear modulus of the DEAP, and the shape coefficient $H = h/(r_1 + r_2)\ln(r_1/r_2)$

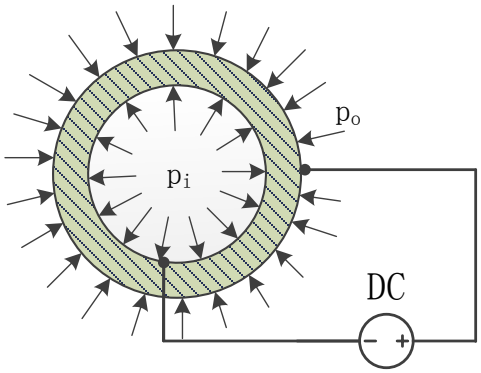

Figure 3. The cross-section of the DEAP ring in the applied electric field.

3. Transfer matrix (TM) theory

The calculation model of the IPC structure is illustrated in Figure 4. With reference to Figure 4(a), an infinite Euler-Bernoulli beam is now periodically attached with 2DOF LR structures. For each unit cell with a lattice constant *a* as shown in Figure 4(b), the DEAPs along with Cu strips constitute an oscillator. Thus one LR oscillator consists of two springs *k* and one mass *m*.

The governing differential equation for free flexural vibration of an Euler-Bernoulli beam can be obtained by [16]:

$$\frac{\partial^2}{\partial x^2}\left[EI\frac{\partial^2 y(x,t)}{\partial x^2}\right]+\rho A\frac{\partial^4 y(x,t)}{\partial x^4}=0 \tag{19}$$

where ρ and E are the density and Young's modulus of the beam respectively; A and I are the cross-section area and the moment of inertia with respect to the axis perpendicular to the beam axis respectively; and $y(x,t)$ is the dynamic displacement at x.

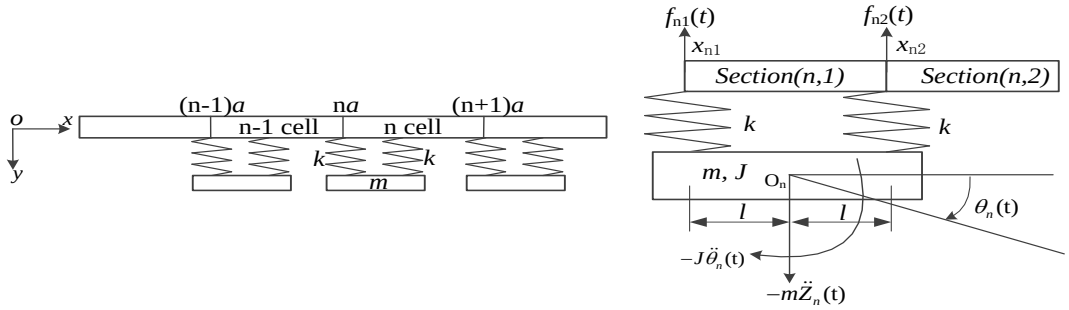

(a) (b)

Figure 4. The calculation model of the IPC structure: (a) the 2DOF LR structures periodically attached on an infinite Euler-Bernoulli beam; (b) the force equilibrium in the *n*th unit cell.

For time harmonic motion of the form $\exp(i\omega t)$, the displacement $y(x,t)$ may be assumed $y(x,t)=Y(x)\exp(i\omega t)$, where ω is the angular frequency and the amplitude $Y(x)$ given by

$$Y(x)=A\cos(\lambda x)+B\sin(\lambda x)+C\cosh(\lambda x)+D\sinh(\lambda x) \tag{20}$$

where $\lambda^4=\rho A\omega^2/EI$.

Each unit cell is divided into two sections. For the *n*th cell as shown in the Figure 4(b), the amplitude at the first section is given by

$$Y_{n1}(x')=A_{n1}\cos(\lambda x')+B_{n1}\sin(\lambda x')+C_{n1}\cosh(\lambda x')+D_{n1}\sinh(\lambda x') \tag{21}$$

where $x'=x-na$, $na\le x\le na+2l$. Similarly, the amplitude at the second section can be written as

$$Y_{n2}(x'')=A_{n2}\cos(\lambda x'')+B_{n2}\sin(\lambda x'')+C_{n2}\cosh(\lambda x'')+D_{n2}\sinh(\lambda x'') \tag{22}$$

where $x''=x-na$, $na+2l\le x\le(n+1)a$.

For the *n*th oscillator, applying the equilibrium conditions of the shear force and the moment about the center of the gravity O_n, gives [17]

$$-f_{n1}(t)-f_{n2}(t)-m\ddot{Z}_n(t)=0\ ,\ f_{n1}(t)(O_n-x_{n1})-J\ddot{\theta}(t)-f_{n2}(t)(x_{n2}-O_n)=0 \tag{23}$$

where $f_{n1}(t)$, $f_{n2}(t)$ are the interactive forces between the oscillator and the beam at the two attachment points x_{n1} and x_{n2}, respectively; m and J are the mass and mass moment of inertia of the oscillator, respectively; the displacement of the *n*th LR oscillator at the center of gravity, $Z_n(t)=V_n exp(i\omega t)$ with V_n being the displacement amplitude; and the torsional displacement of the *n*th oscillator $\theta_n(t)=\alpha_n exp(i\omega t)$ with α_n being the rotational angle.

The forces $f_{n1}(t)$ and $f_{n2}(t)$ are given by

$$\begin{aligned} f_{n1}(t) &= k\left[Z_n(t) - y(x_{n1},t) - (O_n - x_{n1})\theta(t)\right] \\ &= k\left[V_n - Y_{n1}(x_{n1}) - l\alpha_n\right]\exp(i\omega t) \\ &\equiv F_{n1}\exp(i\omega t) \end{aligned} \tag{24}$$

and

$$\begin{aligned} f_{n2}(t) &= k\left[Z_n(t) - y(x_{n2},t) - (x_{n1} - O_n)\theta_n(t)\right] \\ &= k\left[V_n - Y_{n2}(x_{n2}) + l\alpha_n\right]\exp(i\omega t) \\ &\equiv F_{n2}\exp(i\omega t) \end{aligned} \tag{25}$$

respectively. Substituting Eqs. (24), (25) into (23) leads to

$$V_n = k\frac{Y_{n1}(x_{n1}) + Y_{n2}(x_{n2})}{2k - m\omega^2},\ \alpha_n = kl\frac{Y_{n1}(x_{n1}) - Y_{n2}(x_{n2})}{J\omega^2 - 2kl^2} \tag{26}$$

where 2*l* is the distance between the two attachment points x_{n1} and x_{n2},i.e., the length of the strip.

Setting x_{n1}=0 in Eq. (21) and x_{n2}=2*l* in Eq. (22), one can obtain

$$Y_{n1}(x_{n1}) = Y_{n1}(0) = A_{n1} + C_{n1} \tag{27}$$

$$Y_{n2}(x_{n2}) = Y_{n2}(2l) = A_{n2}\cos(2\lambda l) + B_{n2}\sin(2\lambda l) + C_{n2}\cosh(2\lambda l) + D_{n2}\sinh(2\lambda l) \tag{28}$$

These results are now used to derive the dispersion relationship of the Euler-Bernoulli beam with 2DOF LR structures considered.

At the attachment point x_{n2}, (i.e., $x=na+2l$), equations expressing continuity conditions of the displacement and slope, and equilibrium conditions of the bending moment and shear force are given by

$$Y_{n1}(2l) = Y_{n2}(2l)\ ,\ Y'_{n1}(2l) = Y'_{n2}(2l)\ ,\ EIY''_{n1}(2l) = EIY''_{n2}(2l)\ ,\ EIY'''_{n1}(2l) = EIY'''_{n2}(2l) - F_{n2} \tag{29}$$

Substituting Eqs. (21), (22), (24) and (25) into Eq. (29), one can obtain the following relation in compact form by

$$\mathbf{K_1}\boldsymbol{\psi}_{n2} = \mathbf{H}_1\boldsymbol{\psi}_{n1} \tag{30}$$

where $\boldsymbol{\psi}_{n2}=[A_{n2}\ B_{n2}\ C_{n2}\ D_{n2}]^T$ and $\boldsymbol{\psi}_{n1}=[A_{n1}\ B_{n1}\ C_{n1}\ D_{n1}]^T$.

Similarly, at the attachment point x_{n1}, (i.e., $x=na$), the four equations expressing continuity and equilibrium are

$$Y_{(n-1)2}(2l) = Y_{n1}(2l),\quad Y'_{(n-1)2}(2l) = Y'_{n1}(2l)\ ,\ EIY''_{(n-1)2}(2l) = EIY''_{n1}(2l)\ ,\ EIY'''_{(n-1)2}(2l) = EIY'''_{n1}(2l) - F_{n1} \tag{31}$$

Thus, one can obtain

$$\mathbf{K}_2\boldsymbol{\psi}_{n1} + \mathbf{K}_3\boldsymbol{\psi}_{n2} = \mathbf{H}_2\boldsymbol{\psi}_{(n-1)2} \tag{32}$$

Combining Eqs. (30) and (32), the relationship between the *n*th cell and (*n*−1)th cell is given by

$$\boldsymbol{\psi}_{n2} = \mathbf{T}\boldsymbol{\psi}_{(n-1)2} \tag{33}$$

where the transfer matrix $\mathbf{T} = \mathbf{K}_1^{-1}\mathbf{H}_1\left[\mathbf{K}_2 + \mathbf{K}_3\mathbf{K}_1^{-1}\mathbf{H}_1\right]^{-1}\mathbf{H}_2$.

Based on the Bloch dispersion relationship [5] of a periodic structure of infinite length, one can obtain

$$\boldsymbol{\psi}_{n2} = e^{iqa}\boldsymbol{\psi}_{(n-1)2} \tag{34}$$

where q is the Bloch wavenumber in the x direction. Combining Eqs. (33) and (34), one can obtain the eigenvalues (i.e., the Bloch wavenumber q) of the transfer matrix by finding the roots of the determinant

$$\left|\mathbf{T} - e^{iqa}\mathbf{I}\right| = 0 \tag{35}$$

where **I** is the 4×4 unit matrix. It is noted that the imaginary part of the wavenumber governs the wave attenuation. This suggests flexural waves are largely attenuated at the frequencies where a wavenumber q has an imaginary part. Therefore, the structures proposed exhibits a BG property at these frequencies [2].

4. Simulation results

To clarify the mechanism of the BG formation, damping is neglected in the analysis. The IPC structure with nine oscillators is considered for low frequency attenuation and the transmission FRF of the flexural vibration is obtained using the FE technique in the framework of Comsol Multiphysics [1]. Referring to Figure 2, the outer Cu layer is divided into several strips with parameters b denoting the angle of each strip and g the separation angle. In terms of the transmission FRF, the effects of the configuration of the Cu strips are now studied in this section. The dimension parameters are chosen as b=23.3°, 35°, 70°, and g=6.7°, 10°, 20° to ensure $b/(b+g)$=0.78 in each Cu layer. The material parameters for this structure are ρ_{Al}=2700kg/m^3, E_{Al}=7×10^{10}Pa, G_{Al}=2.7×10^{10}Pa, ρ_{DEAP}=1190kg/m^3, E_{DEAP}=5×10^{6}Pa, G_{DEAP}=1.7×10^{6}Pa, ρ_{Cu}=8700kg/m^3, E_{Cu}=1.1×10^{10}Pa, and G_{Cu}=4.1×10^{9}Pa. Other parameters are the same as listed in section 2.

In the simulations, the beam is excited at one end with an acceleration av_1 and the frequency of interest is below 1000Hz. The response at the other end av_2 can be calculated and the transmission FRF is represented in logarithmic scale 10×lg(av_2/av_1).

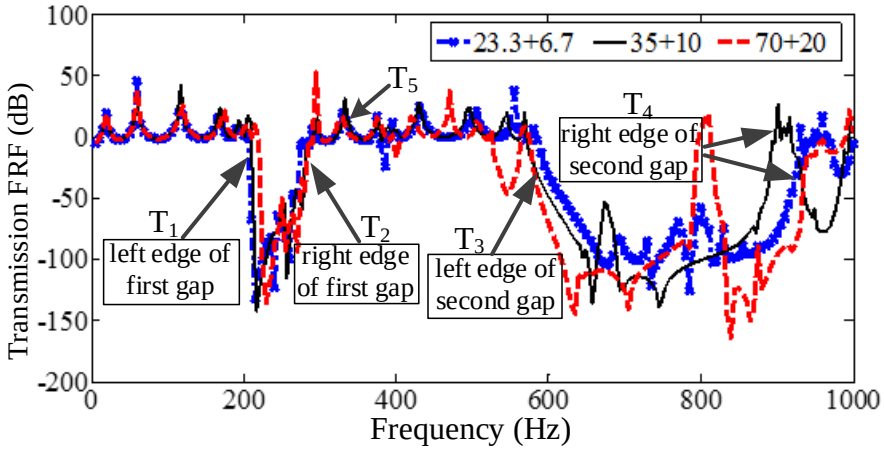

Figure 5. Transmission FRF for the IPC structure with nice unit cells. The parameters of each layer of Cu strips are b=23.3°, g=6.7° (-x-); b=35°, g=10° (—); b=70°, g=20°(---).

The following observations are based on the transmission FRF as plotted in Figure 5:

(1) For each configuration of the Cu layer, it is clear that two BGs are obtained below 1000Hz. This suggests that flexural vibration can be effectively attenuated in the low frequency BG by using the novel design of the Euler-Bernoulli beam attached with discrete Cu strips.

(2) The BGs are largely affected by the configuration of the Cu layer in each cell. The first BG shifts slightly towards lower frequencies with an increasing number of Cu strips. In contrast, the transmission FRF becomes erratic close to 1000Hz. Nevertheless, the general trend is that a broader BG can be achieved by adopting more Cu strips with the lower BG edge less sensitive to the configuration.

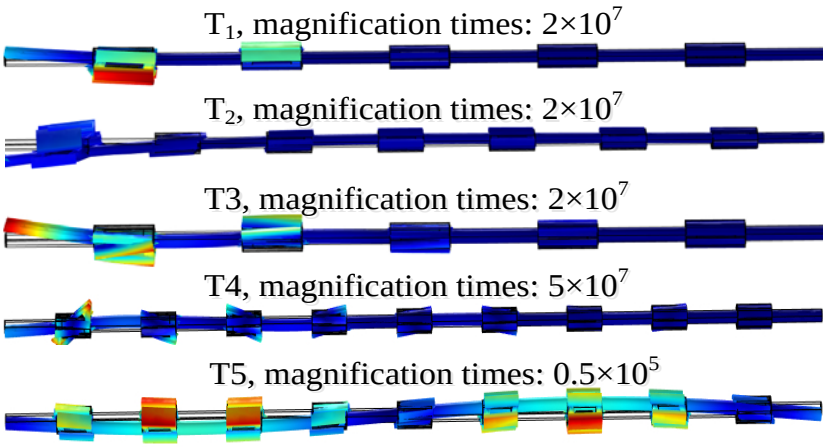

Figure 6. Vibration patterns of the IPC structure at different frequencies.

T_1, T_2, T_3, T_4 are the four BG edges and T_5 is the frequency outside the BG.

For the IPC structure proposed as shown in Figure 5, Figure **6** shows the vibration patterns at the BG edges (T_1, T_2, T_3, T_4) along with one of the vibration patterns outside the BGs (T_5). It is apparent from the figure that for T_1 and T_2 of the first BG, the vibration direction of Cu strips is vertical to the beam. At ω=T_1, only a couple of oscillators close to the excitation end exhibit resonant behaviour with amplified magnitudes; at ω=T_2, all the oscillators start vibrating resonantly. At ω=T_3 and ω=T_4 of the second BG, however, each Cu strip vibrates like a teeter-totter, as a result of the moment of the Cu strips. Similar to the first BG, at ω=T_3, only the first two oscillators have triggered resonant vibrations, while all nine oscillators demonstrate resonant behaviour at ω=T_4. Clearly, flexural vibrations are largely attenuated by passing through the IPC structure at the frequencies of the two BG edges. In contrast, as anticipated, it can be seen form the figure that the flexural vibration at frequencies beyond the BGs, such as ω=T_5, cannot be largely controlled by passing through the IPC structure since the LR structures in each unit cell are inactive for 'absorbing' the energy at these frequencies.

The particular configuration of the Cu layer with b=35° and g=10° is now chosen to study the effect of the voltage on the BGs. As derived in Section 2, the voltage V is related to the dimension variations of DEAP Δr and Δh by Eqs. (14) and (17), and hence the stiffness k given by Eq (18). These relationships are plotted in Figure 7.

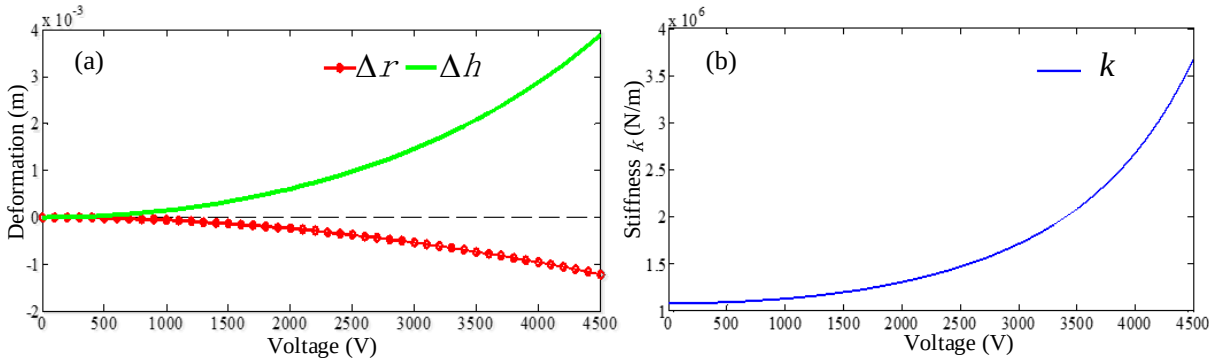

Figure 7. Relationships between the voltage and (a) the deformations Δr, Δh; (b) the stiffness k.

As can be seen from Figure 7(a), the radial thickness of the DEAP ring Δr decreases and the length Δh increases with increasing the applied voltage. Figure 7(b) shows that DEAP becomes stiffer (k increases) under a higher voltage value. The calculated results of Δr, Δh and k at three voltages are listed in Table 1. The transmission FRFs under voltages of 2000V, 3000V, 4000V are illustrated in Figure 8 and the BG edges are shown in Table 2.

Table 1. Results of Δr, Δh and k at different voltages

	Δr (m)	Δh (m)	k (N/m)
2000V	-2.4×10^{-4}	6×10^{-4}	1.31×10^{6}
3000V	-5.4×10^{-4}	1.46×10^{-3}	1.71×10^{6}
4000V	-9.6×10^{-4}	2.88×10^{-3}	2.53×10^{6}

The transmission FRF under voltage of 2000V, 3000V, 4000V is illustrated in Figure 8. Detailed frequencies at edges of both gaps are described in Table 2.

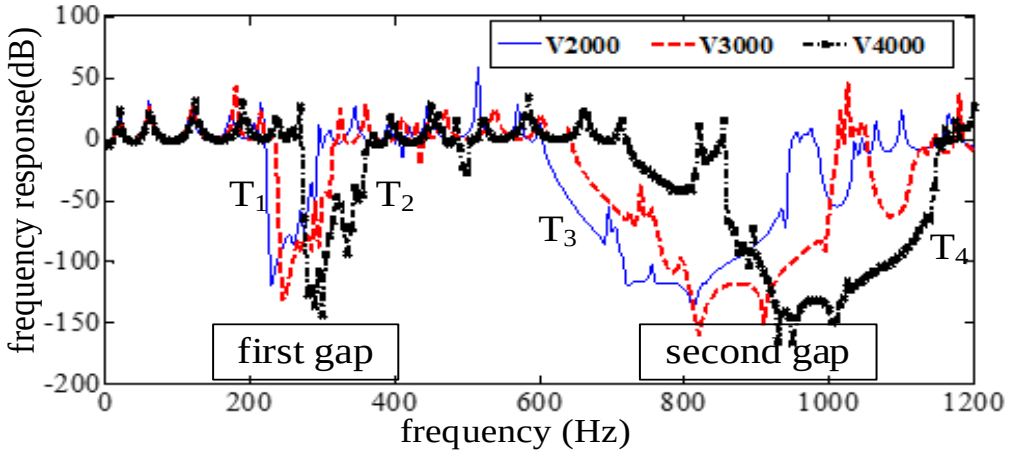

Figure 8. Transmission FRF under the applied voltages of 2000V, 3000V and 4000V.

Table 2. Results of the BG edges

	T_1	T_2	T_2-T_1	T_3	T_4	T_4-T_3
2000V	220Hz	295Hz	75Hz	605Hz	945Hz	340Hz
3000V	235Hz	320Hz	85Hz	645Hz	1015Hz	370Hz
4000V	270Hz	365Hz	95Hz	715Hz	1150Hz	435Hz

Figure 8 shows that both BGs shift toward higher frequency with an increasing voltage. The reason for this that, the applied voltage increases the stiffness of DEAP k, as shown in Figure 7(b), which thereby leads to an increment of the resonant frequency corresponding to each oscillator. Thus the BGs occur at higher frequencies. Moreover, as illustrated in Table 2, a higher voltage leads to wider BGs.

5. Conclusions

In this paper, a novel design of an IPC is proposed for the control of the flexural vibration. The DEAP rings attached with discrete Cu strips acting as oscillators are adopted in each unit cell. This design is particular suitable for the deformation of DEAPs subjected to an electric field. The dispersion relationship is derived based on the TM theory. Simulation results have shown that the LR BGs occur at low frequencies below 1000Hz. In addition, tunable BGs can be realized by changing the applied voltages. It has also been found that a wider BG can be achieved and shifts towards higher frequencies with an increasing applied voltage. The theoretical investigations with numerical calculations provide a framework for the design of the IPC structure for vibration control at low frequencies. Further experimental work will be conducted to evaluate the performance of the structure for flexural wave attention.

Acknowledgments

This work was supported by the National Natural Science Foundation of Chian within Grant No. 51303209.

References

[1] Zhao X, Shuai C. Application review of dielectric electroactive polymers (DEAPs) in phononic crystals. In: Editor, editor The 7th International Congress on Vibration Engineering; 2015. Pub Place; 2015.

[2] Yu D, Liu Y, Zhao H, Wang G, Qiu J. Flexural vibration band gaps in Euler-Bernoulli beams with locally resonant structures with two degrees of freedom. *Phys Rev B*. 2006;**73**(6):64301.

[3] Kushwaha M S HPDL. Acoustic band structure of periodic elastic composites. *Phys. Rev. Lett.* 1993;**71**(13):2022-5.

[4] Zhou X, Chen C. Tuning the locally resonant phononic band structures of two-dimensional periodic electroactive composites. *Physica B*. 2013;**431**:23-31.

[5] Xiseng W, Jihong W, Dianlong Y, Gang W. Phononic Crystals.: National Defense Industry Press; 2009.

[6] Liu ZY, Zhang X, Mao Y. Locally resonant sonic materials. *Science*. 2000;**289**:1734-6.

[7] Gei M, Roccabianca S, Bacca M. Controlling Bandgap in Electroactive Polymer-Based Structures. *ASME TRANSACTIONS ON MECHATRONICS*. 2011;**16**(1):102-7.

[8] Gal Shmuela GD. Band-gaps in electrostatically controlled dielectric laminates subjected to incremental shear motions. *J Mech Phys Solids*. 2012;**60**:1970-81.

[9] Yang W, Chen L. The tunable acoustic band gaps of two-dimensional phononic crystals with a dielectric elastomer cylindrical actuator. *Smart Mater. Struct.* 2008;**17**.

[10] Shmuela G. Electrostatically tunable band gaps in finitely extensible dielectric elastomer fiber composites. *Int J Solids Struct*. 2013;**50**:680-6.

[11] Kim KJ, Tadokoro S. Electroactive Polymers for Robotic Applications Artificial Muscles and Sensors.: Springer; 2007.

[12] Pelrine R, Kornbluh R, Jeseph JP. *Sensors and Actuators A*. 1999;**64**:77.

[13] Carpi F, Rossi D. Dielectric elastomer cylindrical actuators: electro-mechanical modeling and experimental valuation. *Materials Science & Engineering C*. 2004;**24**:555-62.

[14] Timoshenko SP, Goodier JN. Theory of Elasticity. New York: McGraw-Hill ; 1986.

[15] Zhao SC. *Chin. Mech. Eng*. 2001;**15**:962.

[16] Timoshenko S, Young DH, Weaver W. Vibration Problems in Engineering. Wiley, New York; 1974.

[17] Bradley CE. *J Acoust Soc Am*. 1994;**96**:1854.